Nanoscale Horizons

ROYAL SOCIETY OF CHEMISTRY

REVIEW

View Article Online
View Journal | View Issue

Cite this: *Nanoscale Horiz.*, 2025, **10**, 681

Semiconductor photocatalytic antibacterial materials and their application for bone infection treatment

Ruizhong He,†[a] Yulong Gu,†[a] Jiye Jia,[a] Feng Yang,[a] Ping Wu,[b] Pei Feng *[a] and Cijun Shuai *[ac]

Bacterial infection in bone tissue engineering is a severe clinical issue. Traditional antimicrobial methods usually cause problems such as bacterial resistance and biosecurity. Employing semiconductor photocatalytic antibacterial materials is a more controlled and safer strategy, wherein semiconductor photocatalytic materials generate reactive oxygen species under illumination for killing bacteria by destroying their cell membranes, proteins, DNA, *etc.* In this review, P-type and N-type semiconductor photocatalytic materials and their antibacterial mechanisms are introduced. Type II heterojunctions, P–N heterojunctions, type Z heterojunctions and Schottky junctions have been reported to reduce the recombination of carriers, while element doping, sensitization and up-conversion luminescence expand the photoresponse range. Furthermore, the applications of semiconductor photocatalytic antibacterial materials in bone infection treatment such as osteomyelitis treatment, bone defect repair and dental tissue regeneration are summarized. Finally, the conclusion and future prospects of semiconductor photocatalytic antibacterial materials in bone tissue engineering were analyzed.

Received 22nd October 2024,
Accepted 10th January 2025

DOI: 10.1039/d4nh00542b

rsc.li/nanoscale-horizons

1. Introduction

Bone infection caused by traumatic fracture, surgical infection, blood transmission, adjacent tissue infection and immune dysfunction cannot be ignored, and its incidence is as high as 30%.[1] These infections often lead to serious complications such as osteomyelitis and osteonecrosis, which affect the quality of life of patients and even threaten their lives. Implant-associated infections, in particular, have become a growing problem with the popularity of orthopedic surgery and artificial joint replacement.[2] Implant infection can not only lead to postoperative complications, but also to implant failure, bone damage and even reoperation, and it is thus difficult to treat and require a long course of treatment.[3] Since penicillin was discovered in 1928, various antibiotics have been used to cope with bacterial infection, such as vancomycin, tetracycline, and ciprofloxacin.[4] For example, Ren *et al.*[5] found that bisphosphonate-bound sitafloxacin combined with vancomycin was effective in clearing methicillin-resistant *Staphylococcus aureus* (MRSA) infection, reducing bone resorption and biofilm formation from the surrounding implant. However, the abuse of antibiotics generates bacterial resistance, which can lead to the production of super bacteria, and long-term or high doses of antibiotics may cause damage to liver and kidney functions. Therefore, there is an urgent need to find a strategy to replace antibiotics and fight bacterial infection.

To deal with the problem of bacterial infection without causing bacterial resistance, researchers have sought to use other strategies to combat bacteria, such as metal ion release, photothermal therapy (PTT), and antibacterial gas therapy. Shicheng *et al.*[6] prepared Cu-doped bioactive glass using electrophoretic deposition to deal with implant-associated infection, and the released Cu ions could improve the antibacterial effect of the implant through contact killing, immune regulation, and other functions. Although released metal ions have excellent antibacterial effects, they also exhibit a certain cytotoxicity, which limits their application in bone tissue engineering. By contrast, PTT has no cytotoxicity and can be controlled by near-infrared (NIR) light; for example, Zhang *et al.*[7] modified a nucleic acid aptamer on the surface of a polycaprolactone (PCL) nanofiber scaffold to generate mild hyperthermia through NIR light irradiation, thus effectively preventing the proliferation of bacteria in the early stage of bone defect repair. To completely kill bacteria, the temperature of photothermal

[a] *State Key Laboratory of Precision Manufacturing for Extreme Service Performance, College of Mechanical and Electrical Engineering, Central South University, Changsha 410083, China. E-mail: fengpei@csu.edu.cn, shuai@csu.edu.cn*
[b] *School of Traditional Chinese Medicine, Hunan University of Chinese Medicine, Changsha 410208, China*
[c] *Jiangxi Province Key Laboratory of Additive Manufacturing of Implantable Medical Device, Jiangxi University of Science and Technology, Nanchang 330013, China*
† These authors contributed equally to this work.

therapy is usually maintained at >50 °C, but excessive temperature could also cause damage to surrounding healthy tissue. Antibacterial gases are able to diffuse freely into biofilms and exert an antibacterial effect within bacterial cell due to their low molecular weight, but the controllability of the gas release rate and cytotoxicity need further consideration.

As a burgeoning antibacterial strategy, photocatalytic antibacterial effect has attracted increasing attention. Specifically, photocatalytic antibacterial materials can produce electrons and holes because the electron can jump from the valence band (VB) to the conduction band (CB) under illumination. Then, the produced electrons and holes can react with substances such as water and oxygen to produce reactive oxygen species (ROS) with strong redox properties, and the ROS can kill bacteria by destroying the cell membranes, proteins, DNA, and so on. The generation of ROS in photocatalytic antibacterial processes can be precisely controlled by the external illumination, which is a key advantage of this method.[8] Once the bacteria are eliminated, the external light source can be turned off, effectively halting the production of ROS and preventing any potential damage to normal, healthy cells.[9] This ability to control the activation of ROS based on illumination makes photocatalytic antibacterial treatment a safer, more targeted, and more controlled strategy compared to traditional antimicrobial methods, which may suffer from issues such as toxicity to surrounding tissues and bacterial resistance.[10] This control over ROS generation offers a promising approach for localized, selective bacterial eradication without causing harm to the host cells. Semiconductor photocatalytic materials are widely used to combat bacterial infection in bone tissue engineering but only a few articles have summarized their application in bone tissue engineering.

In this review, the research progress on semiconductor photocatalytic antibacterial materials and their application in bone tissue engineering have been presented. It focuses on advancements made during the period 2019–2024, with key topics including semiconductor, photocatalysis, antibacterial, heterojunctions, doping, up-conversion, bone repair, bone scaffolds, tooth implants, and osteomyelitis. The application of semiconductor materials in bone repair has gradually become a hot research direction, and breakthroughs in related technologies have provided new solutions for bone regeneration and repair. This paper will systematically review the advances in these research fields, analyze their challenges and development trends, and provide references for the future application of related technologies. Two types of semiconductor photocatalytic materials are introduced, namely, P-type semiconductor and N-type semiconductor, and the advantages and limitations of each material have been discussed. To decrease the recombination of electrons and holes, some methods that could separate electrons and holes were summarized, such as type II heterojunction, P–N heterojunction, type Z heterojunction and Schottky junction. To increase the utilization of light, some strategies that could expand the light response range have been summarized, such as element doping, sensitization and up-conversion luminescence. Furthermore, the applications of semiconductor photocatalytic antibacterial materials in bone tissue engineering have been discussed, such as osteomyelitis treatment, bone defect repair and dental tissue regeneration. Finally, the prospects and challenges of semiconductor photocatalytic antibacterial materials in bone tissue engineering have been summarized.

2. Semiconductor photocatalytic materials

Bacterial infection in bone tissue engineering has always been a difficult problem. However, the development of semiconductors has provided a new solution for it in recent years. The band structure of a semiconductor typically features a low-energy VB filled with electrons and an empty high-energy CB, and the distance between these two regions is called the band gap width. The band gap in semiconductors is usually discontinuous, and their photocatalytic behavior depends on the specific band structure. When light energy matches or exceeds the band gap, electrons in the VB are excited to the CB, moving to the surface and creating holes in the VB, resulting in a highly active pair of hole–electrons, which can also be called photogenerated carriers. The electrons in the CB react with oxygen molecules (O_2) in solution to form the superoxide anion ($^{\bullet}O_2^-$) through the equation $e^- + O_2 \rightarrow {}^{\bullet}O_2^-$.[11] The holes in the VB react with hydroxide ion (OH^-) to form the hydroxyl radical ($^{\bullet}OH$) ($h^+ + OH^- \rightarrow {}^{\bullet}OH$).[12] Besides, $^{\bullet}O_2^-$ can further react with water molecule to form the hydrogen peroxide (H_2O_2) ($^{\bullet}O_2^- + H_2O \rightarrow H_2O_2 + OH^-$).[13] These ROS have strong redox properties, and when they come into contact with bacteria, they can destroy the bacteria cell membrane, proteins and DNA, thus leading to bacterial death. Semiconductor materials can be divided into P-type and N-type semiconductors according to their carriers, and commonly used semiconductor photocatalytic antibacterial materials are shown in Table 1.

2.1. N-Type semiconductor photocatalytic materials

N-Type semiconductors, also known as electronic semiconductors, are semiconductors in which the free electron concentration is significantly higher than the hole concentration.[36] The letter ''N'' comes from the English word ''Negative'', meaning negative electricity. In N-type semiconductors, the main carriers involved in the conductance are negatively charged electrons, which come from the doped donor impurity.[37] Any semiconductor doped with donor impurities, with donor concentration higher than acceptor concentration, is an N-type semiconductor, as shown in Fig. 1(A). The widely used semiconductor photocatalytic antibacterial materials, such as titanium dioxide (TiO_2), zinc oxide (ZnO), graphitic carbon nitride (g-C_3N_4), bismuth sulfide (Bi_2S_3), molybdenum oxide (MoO_3), and layer double hydroxides (LDHs), are mainly introduced in this paper.

TiO_2 antibacterial materials have been widely used in medical devices, dental implants and other medical aspects to control pathogenic bacterial infection, as shown in Fig. 1(B).

Table 1 Commonly used semiconductor photocatalytic antibacterial materials

Type	Materials	Band gap (eV)	Absorption wavelength	Advantage	Drawback	Ref.
N	TiO_2	3.0–3.2	Ultraviolet (UV) light	• Low toxicity • High biocompatibility, • High antibacterial activity	• Broad band-gap • Fast recombination of electron–hole pair	14
	ZnO	3.2–3.7	UV light	• UV resistance • Good photocatalytic performance • Antibacterial activity	• Broad band-gap • Fast recombination of electron–hole pair	15
	g-C_3N_4	2.7	UV light	• Biocompatible • Non-toxic • Low manufacturing cost	• High electron–hole recombination rate • Insufficient absorption of visible light • Low surface area	16
	Bi_2S_3	1.3–1.7	Visible light	• Visible-light response	• Broad band gap • Rapid recombination of holes and electrons	17 and 18
	WO_3	2.7–2.8	UV light	• Non-toxic and stable in water-based media	• High recombination of photogenerated carriers	19 and 20
	WS_2	1.9	Visible light	• Large surface area can increase the active site	• High recombination of photogenerated carriers	21
	ZnS	3.7	UV light	• Antioxidant • Hydrolytic chemical stability	• Broad band-gap • Fast recombination of electron–hole pair	22
	CdS	2.4	Visible light	• Strong reducing ability	• Severe photocorrosion occurs during the photocatalytic reaction	23
	SnS_2	2.0–2.4	Visible light	• High specific surface area and porosity	• Charge mobility difference	24
P	Cu_2O	2.0–2.2	Visible light	• Inhibit the recombination of electron–hole pairs	• Optical instability	25
	CuO	1.2	Visible light	• Low cost • Narrow band gap	• Low photocatalytic activity • Less oxidation activity	26
	CuS	1.7–2.2	Visible light	• Narrow band gap • Good light absorption performance in the visible–NIR region	• Lack of chemical stability • Rapid recombination of photogenerated carriers • Particle aggregation	27
	MoS_2	1.78	Visible light	• Good visible light absorption ability	• A limited number of active edge sites are available	28
	SnS	1.3	NIR	• Narrow band gap • High absorption coefficient	• Low conductivity and poor capacity retention	29
	AgBr	2.57	Visible light	• High photocatalytic efficiency	• Shielding effect by Ag layers on the surface of silver halide	30 and 31
	NiO	3.3	UV light	• Low-cost and earth-abundant	• The active sites to the amorphization-induced under-coordinated Ni atoms would result in electron doping in NiO	32
	CoO	2.44–2.6	Visible light	• High activity • Relatively narrow bandgap	• Lattice distortion (disorder) will produce localized electronic states blocking the carrier migration • Short lifespan	33–35

TiO_2 has three phases, namely, anatase, rutile, and brookite, and it can respond to UV light. At the same time, it has high antibacterial activity and has been widely used in the field of photocatalysis. Many researchers have studied TiO_2 antibacterial materials and their antibacterial effects.[41–43] Xiao *et al.*[44] constructed FeS_2-sensitized TiO_2 materials *via* a hot-solvent method, and the disinfection efficiency was 95.7% and 92.4% for *Escherichia coli* (*E. coli*) and *Staphylococcus aureus* (*S. aureus*), respectively. Varnagiris *et al.*[45] deposited TiO_2 films on polystyrene magnetic beads by magnetron sputtering technology. Under ultraviolet irradiation, TiO_2 films produced many ROS and the results indicated that 94% of *E. coli* was killed by the films. Additionally, the photocatalytic antibacterial properties of TiO_2 were largely influenced by the cell wall structure. For optimal photocatalytic inactivation, direct contact between bacteria and the TiO_2 surface is vital as it increases the likelihood of ROS attack. Consequently, photocatalytic antibacterial effectiveness depends on cell wall thickness, cell envelope morphology, and the outer membrane's resistance to ROS from the photocatalyst.[46] Besides, the development of TiO_2 faces key problems such as wide semiconductor energy band, low quantum efficiency, and inability to produce visible light response, which limits its application in bone tissue engineering. How to improve these shortcomings of semiconductors is the key to using TiO_2 photocatalytic antibacterial materials.[47]

As a multifunctional biosafety material, ZnO has outstanding UV resistance, good photocatalytic properties and antibacterial activity, and has shown broad practical application prospects in research and development, as shown in Fig. 1(C). Some studies have pointed out that the antibacterial effect of ZnO comes from the production of ROS, the release of Zn^{2+} and cell membrane damage. Many studies clearly show that ZnO nanoparticles could produce ROS, including $^{\bullet}O_2^-$, H_2O_2 and hydroxyl radicals ($^{\bullet}OH$), which could lead to bacterial death. Moreover, due to the oxidizing ability of Zn^{2+} released by ZnO, Zn^{2+} interacts with organic functional groups and

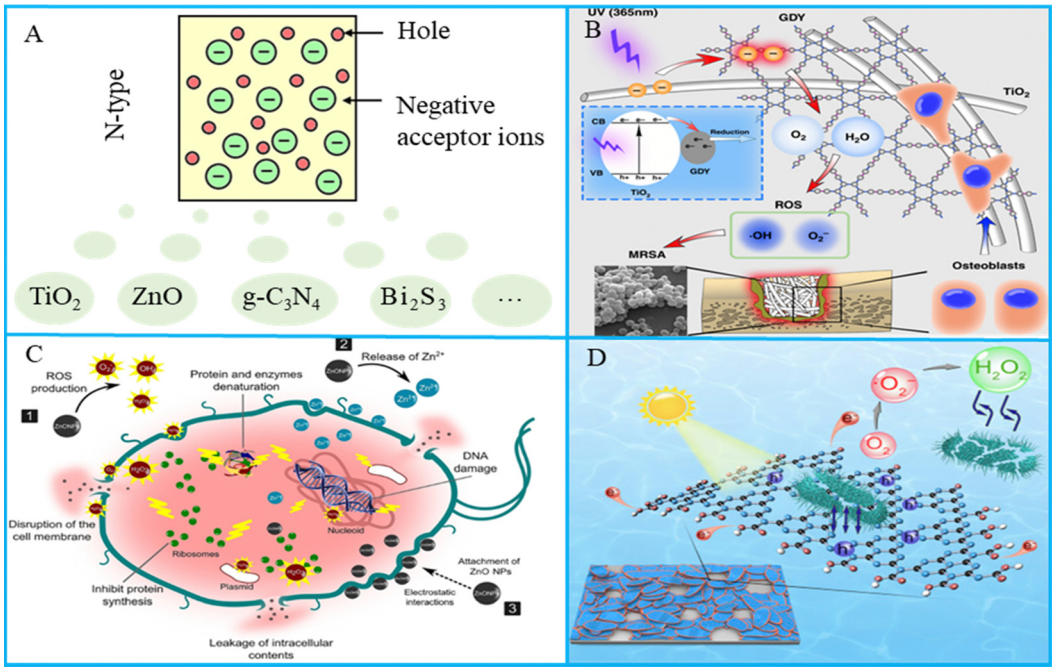

Fig. 1 (A) N-Type semiconductors with electrons as the main photocarriers. (B) Schematic of graphdiyne-modified TiO_2 nanofibers with osteoinductive and enhanced photocatalytic antibacterial activities to prevent implant infection. Reproduced with permission.[38] Copyright 2020, Springer Nature. (C) Schematic illustration of the antimicrobial mechanism of ZnO NPs against bacterial cells. Reproduced with permission.[39] Copyright 2019, Springer Nature. (D) Schematic diagram of indirect bacteria inactivation using H_2O_2 generated by an edge-functionalized g-C_3N_4 nanosheet. Reproduced with permission.[40] Copyright 2019, Elsevier.

attaches to bacterial cells and membrane proteins. It penetrates bacterial cells, disrupting their electron transfer system and hindering protein gene expression. Nonato *et al.*[48] prepared poly-lactic acid (PLA) bone scaffold with ZnO nanofibers, and the results showed that ZnO nanofibers exhibited good antibacterial properties. The specific surface area of ZnO will affect its antibacterial effect, and small size ZnO particles and high specific surface area ZnO have better antibacterial effect.[49] Besides, ZnO is a promising antimicrobial agent; however, it only reacts with UV light due to its wide bandgap. In addition, ZnO exhibits rapid electron–hole pairs recombination, which limits its photocatalytic antibacterial efficiency.

g-C_3N_4 is a commonly used photocatalytic material with good biosafety and excellent photocatalytic effect, and it has been used in many fields such as antibacterial, water decomposition and carbon dioxide decomposition. An example of antibacterial application of g-C_3N_4 is shown in Fig. 1(D). Liu *et al.*[50] prepared nitrogen-deficient g-C_3N_4 ultra-thin nanosheets using thermal polymerization technology. The results indicated that the nanosheets could reduce O_2 to $^{\bullet}O_2^-$, which could attack the cell membrane of *E. coli*. Guo *et al.*[51] prepared acridinium-grafted g-C_3N_4 nanosheets, which changed the band gap of g-C_3N_4 from 2.77 eV to 2.12 eV. Molecular dynamics simulation reveals that the nanosheets could insert the bacteria, which facilitated ROS combination with the bacterial cell membrane, and the removed biofilm biomass was 91% after light irradiation. g-C_3N_4 has the excellent photocatalysis effect similar to TiO_2, but the chemical potential of VB is lower than that of $^{\bullet}OH$ generation, causing low generation rate of $^{\bullet}OH$, and the antibacterial effect of $^{\bullet}O_2^-$ is lower than $^{\bullet}OH$, which limits its antibacterial application.

Bi_2S_3 is a layered semiconductor with a narrow band gap of 1.2–1.7 eV.[52] It has good photocatalytic stability, low cost, harmless to human body, and is an excellent choice for bone tissue engineering antibacterial materials. Wang *et al.*[50] prepared urchin-shaped Au/Bi_2S_3 nanomaterials by the hard template method to replace antibiotics and combat superbugs. Au/Bi_2S_3 core–shell structure improved the separation of electron–hole pairs and increased the efficiency of ROS production. As a result, the bactericidal rate of *S. aureus* and *E. coli* reached 100% under NIR irradiation. Wang *et al.*[53] developed a green and reliable antimicrobial method by loading ZnS and Bi_2S_3 into thermally-sensitive polymer microspheres. The Bi_2S_3 could be released under the NIR irradiation because the microspheres transformed the absorbed NIR into heat and the thermally-sensitive polymer could be melted when the temperature was above the fusing point, and compared with the photothermal method alone, the killing rates of *S. aureus* and *E. coli* were increased remarkably. Although the Bi_2S_3 can be excited under NIR, the narrow band gap also corresponds to low redox potential, thus limiting the generation of ROS.

MoO_3, as a typical 2D layer structure material, shows remarkable photocatalytic and antibacterial properties.[54] Recently, there has been extensive research on the use of MoO_3 nanomaterials for photodynamic or photocatalytic antibacterial applications. Gao *et al.*[55] prepared an oxygen vacancy-

mediated bactericidal MoO_3, and MoO_3 nanosheets were able to activate the adsorbed oxygen production $^{\bullet}O_2^-$, break the cell membrane of the bacteria attached to the surface, and induce the production of intracellular ROS, resulting in the death of the bacteria, and the antibacterial rate reached 99% in bacterial disinfection of authentic atmosphere. Yang *et al.*[56] anchored MoO_3 nanosheets to the surface of carbon nanosheets, which effectively collected NIR light and promoted the transfer of charge carriers, thus greatly enhancing the ability of $^{\bullet}O_2^-$ generation. After 50 min of NIR light treatment, folds and partially merged membranes appeared on the surface of the bacterial cells, and eventually the violent collapse of the cell structure led to the death of the bacteria.

LDHs are an important class of layered materials, which are classified as a type of semiconductor material, known as naturally occurring hydrotalcite compounds, and they have been widely utilized in the fields of photocatalytic antibacterial materials and bone repair.[57] Rad *et al.*[58] synthesized FeCuMg and CrCuMg LDHs and compared their sonophotocatalytic activities. The bandgap energies of FeCuMg and CrCuMg LDHs were calculated to be 2.54 eV and 2.41 eV, respectively. At 600 μg mL^{-1}, CrCuMg LDH and FeCuMg LDH reduced the activity of *S. aureus* by 91.3% and 80.0%, respectively. Mg alloy materials used in biomedicine lack corrosion resistance and antibacterial properties, while LDH surface coating engineering technology is expected to improve their antibacterial effects.[59] Zhang *et al.*[60] prepared a plasma electrolytic oxidation coating on Mg alloy and modified it with LDH. After NIR irradiation, the bacterial colony of the LDH group decreased significantly, indicating that the LDH film had good antibacterial activity. Besides, the sample also had good biocompatibility and osteogenic induction.

2.2. P-Type semiconductor photocatalytic materials

Compared with N-type semiconductors, which use electrons as the main carriers, P-type semiconductors, also known as hole-type semiconductors, refer to semiconductors with positively charged holes as the main conductive carrier or impurity semiconductors with hole concentrations much higher than free electron concentrations.[61] In P-type semiconductors, holes are the majority charge carriers and free electrons are the minority charge carriers. The holes act as positive charge carriers and lead the conduction process.[62] The letter "P" is derived from the first letter of the word "Positive". In this type of semiconductor, the charge carriers involved in the conductivity are mainly positively charged holes, which come from the acceptor in the semiconductor,[63] as shown in Fig. 2(A). In this article, the main introduced P-type semiconductors are CuO, CuS and Mo_2S.

CuO is a monoclinic crystalline semiconductor, and in addition to producing ROS, CuO can also release Cu^{2+} to contact bacteria and destroy bacterial cell membranes;[67] an example diagram of the antibacterial use of CuO photocatalysis is shown in Fig. 2(B). Guan *et al.*[68] found that ROS produced by CuO could destroy bacterial cell structure. Several studies have shown that the shape, morphology, and size of CuO nanostructures appear to influence their antimicrobial properties. Siddiqui *et al.*[64] studied the biosynthesis of flower-shaped CuO

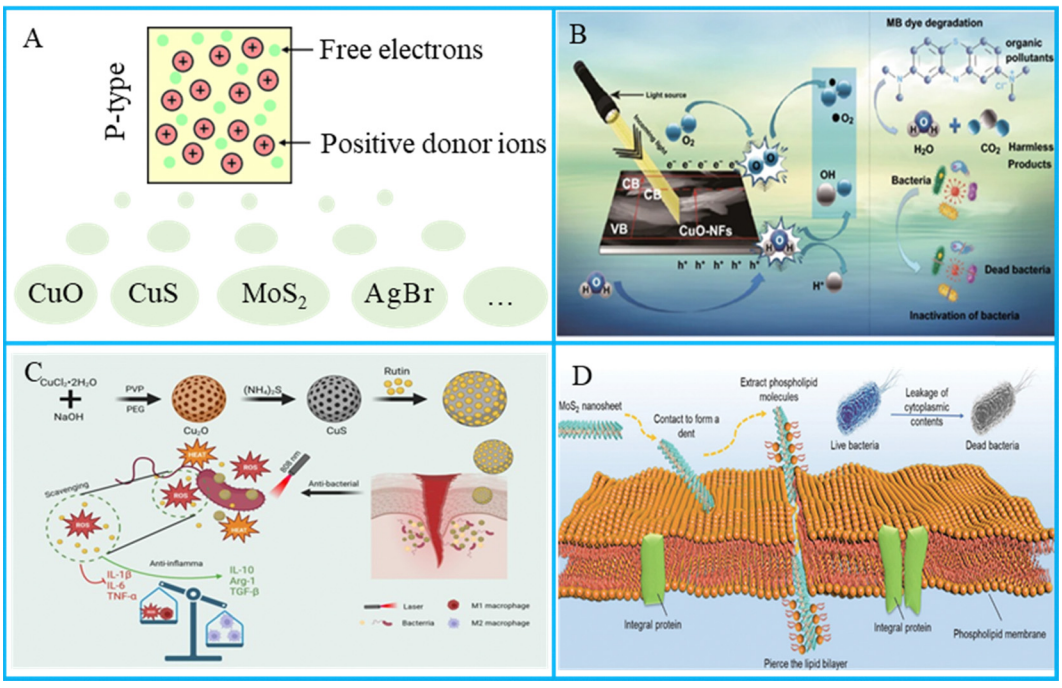

Fig. 2 (A) P-type semiconductors with holes as the main photocarriers. (B) The sustainable performance of CuO in methylene blue degradation and bacterial organisms. Reproduced with permission.[64] Copyright 2020, Springer Nature. (C) Synthesis of CuS/rutin and its antibacterial mechanisms. Reproduced with permission.[65] Copyright 2024, Elsevier. (D) The physical antibacterial mechanisms between MoS_2 nanosheets and bacterial cell membranes. Reproduced with permission.[66] Copyright 2022, John Wiley and Sons.

nanostructures and photocatalytic antibacterial activities, and the obtained results confirmed that the prepared flower-shaped CuO nanostructures showed good antibacterial activity against *E. coli* (29 ± 2 mm) at a concentration of 100 μg mL^{-1}. George *et al.*[69] focused on the effect of calcination temperatures on the size, size distribution and morphology of the prepared CuO nanoparticles. The results showed that CuO nanoparticles calcined at 800 °C had a smaller size and better antibacterial effect.

CuS nanomaterials can excite a large number of charge carriers, which endows the materials with localized surface plasmon resonance properties in the NIR region, as shown in Fig. 2(C). Zou *et al.*[70] used vancomycin (Van)-loaded CuS nanoparticles (CuSNPs) (CuS@Van) for killing the bacteria. In this study, Van was used not only as a reducing agent acting in tandem with CuSNPs but also as a booster to promote CuS to enter the bacterial interior. It was found that CuS@Van had good antibacterial activity and the antibacterial rate was up to 90%. CuS is also useful for bone tissue engineering. Xu *et al.*[71] used 3D printing technology to prepare PCl bone scaffold, and CuS nanoparticles and polyethylene glycol were added to endow the scaffold with antibacterial properties and elasticity. Under NIR treatment, the scaffold showed good antibacterial and bone regeneration ability.

MoS_2 has the greatest potential to fight pathogens because of its layered structure, and the mechanical antibacterial effect is shown in Fig. 2(D). Hu *et al.*[72] modified two-dimensional MoS_2 using galactose and focal ligands as starting materials, which had the ability to selectively locate *Pseudomonas aeruginosa via* polyvalent carbohydrate–lectin interactions. The results showed that ceftazidime antibiotics could be thermally released from two-dimensional MoS_2 when NIR and white light irradiated antibiotic-supported materials, causing intracellular oxidative stress and reducing the level of intracellular glutathione (GSH), resulting in an antimicrobial rate of 90%. Some researchers reported an enhancement in its antibacterial effect by changing the size and form of MoS_2, and MoS_2 quantum dots had better photocatalytic effect than monolayer MoS_2. The yield of singlet oxygen by MoS_2 quantum dots was higher than that of MoS_2 nanosheets and bulk MoS_2. Most importantly, reducing the number of layers changed the band gap of MoS_2, with values of about 1.1–1.7 eV for different number of layers. The results showed that MoS_2 quantum dots had stronger hole and electron redox activity than MoS_2 blocks and MoS_2 nanosheets.

2.3. Size and morphology

The size and morphology of semiconductor photocatalytic materials have significant influence on the photocatalytic effect.[73] The different size and morphology of the material usually affect its specific surface area, and a larger specific surface area can provide more active sites and enhance the efficiency of the photocatalytic reaction.[74] The different size and morphology will affect the light absorption characteristics, electron transport rate and selectivity of the catalytic reaction.[75] By precisely controlling the size and topography, the band structure of the semiconductor material can also be adjusted to further optimize its response to light. Therefore, optimizing the size and morphology of semiconductor photocatalytic materials is a key factor to improve their photocatalytic efficiency.

From the perspective of size, the influence of the size of semiconductor photocatalytic material on its photocatalytic performance is mainly reflected in the specific surface area and quantum effect.[76] As the size decreases, the specific surface area of the material increases, thus providing more active sites for the reaction, which helps to improve the adsorption amount of the reactants and the efficiency of the photocatalytic reaction. Sun *et al.*[77] studied the effect of particle size distribution for the photocatalytic effect of carbon dots, and the smaller particles had significantly enhanced antibacterial activity. Cheng *et al.*[78] constructed MOF/CdS photocatalyst with different specific surface area, and the results indicated that compared with pure CdS and MOF, the MOF/CdS photocatalyst had a larger specific surface area and better photocatalytic effect. In addition, the quantum size effect is particularly significant in nanomaterials. When the material size reaches the nanometer scale, the energy level structure of electrons changes, which can improve the light absorption and electron transition ability so as to improve the efficiency of photocatalytic reaction.[79] Kazemi *et al.*[80] synthesized Se nanoparticles by biosynthesis, which exhibited a band gap of 5.12 eV, different from the bulk (5.2 eV) due to the quantum size effect, and showed enhanced photocatalytic antibacterial activity.

From the perspective of morphology, one-dimensional nanostructures (such as nanowires or nanorods) or two-dimensional nanostructures (such as nanosheets or less lamellar material) can provide more reaction sites and enhance the adsorption capacity of the material due to their larger surface exposure. Liu *et al.*[81] developed an NIR-activated heterostructure catalyst (MXene/Co nanowires) consisting of two-dimensional MXene and one-dimensional Co nanowires for acting against bacteria in drug-free therapy. Heterostructure coatings on orthopedic implants could achieve high antimicrobial efficacy of more than 90% within 20 min. Besides, the nanostructures can also damage bacterial cell membrane by mechanical damage. Zhang *et al.*[82] constructed TiO_2 nanorod arrays in the surface of implant, which could kill the bacteria not only through ROS and heat under NIR but also through the effect of mechanical puncture. Metasurface engineering is a promising strategy for fighting bacterial infections in Ti-based implants. Yang *et al.*[83] produced metasurface with strong NIR response antibacterial activity on Ti alloy implants through a newly invented alkali–acid bidirectional hydrothermal method based on topochemical transformation. The antimicrobial rates of the metasurface-treated Ti against *E. coli* and *S. aureus* were 96.88% and 97.56%, respectively. The powerful nanostructure-induced effect provided a good way to improve the antibacterial effect and bone regeneration effect of implants.

Semiconductor photocatalytic antibacterial materials have good application prospect in bone tissue engineering, but there are some key problems such as broad semiconductor energy

bandwidth, causing failure to produce visible light response and fast electron–hole pair recombination, causing low quantum efficiency. Thus, studies on improving photocatalytic properties are particularly important. Methods to improve the photocatalytic properties mainly include promoting the separation of photogenerated carriers and expanding the light response range.

3. Separation of photogenerated carriers

As mentioned earlier, photocatalytic materials are able to generate electron–hole pairs under light and further generate ROS. However, these electrons and holes do not remain separated forever, and most of the transitioned electrons return to the VB and undergo a recombination process, releasing energy usually in the form of light or heat, resulting in photogenic carriers unable to participate in an effective photocatalytic reaction.[84] Recombination can reduce the photocatalytic efficiency of semiconductor materials, especially in applications such as photocatalytic degradation and antibacterial, where electrons and holes must be effectively separated to generate ROS or drive charge transport.[85] To solve the problem of fast recombination of photogenerated carriers, suitable heterojunctions are usually constructed between semiconductors. It is considered to be a useful strategy for promoting the separation of photogenerated electron–hole pairs and enhancing the photocatalytic activity. According to the different carrier separation mechanisms and coupling materials of various hybrid heterojunctions, semiconductor photocatalysts can be divided into different heterojunctions. In this section, we mainly introduce several commonly used types of heterojunctions and their applications in the field of photocatalytic antibacterial materials, including Schottky junction, type II heterojunction, P–N heterojunction and type Z heterojunction.

3.1. Schottky junction

Semiconductors are able to work with conductive substances such as GO and precious metal nanoparticles to transfer the generated electrons through good electrical conductivity, which is able to reduce the recombination of electrons and holes. At the same time, due to the difference in Fermi energy levels, Schottky barriers, also known as Schottky junction (Fig. 3(A)), are generated between them, which can prevent electron reflux, effectively realize the separation of electrons and holes, and improve the photocatalytic efficiency. Ma *et al.*[86] constructed an oxygen vacancy-embedded LDH/$Ti_3C_2T_x$ MXene 2D/2D sheet-like Schottky heterostructure, which had improved photocatalytic activity. Wang *et al.*[87] encapsulated colloidal semiconductor quantum dots into an MOF matrix using a simple ligation-assisted self-assembly method, which showed excellent antimicrobial properties against *E. coli* (7.99 lg reduction in 60 min) and *S. aureus* (5.23 lg reduction in 120 min) under visible light irradiation. Although semiconductor cooperation with conductive substances is cost-effective and has high optical stability and optical catalytic efficiency, the preparation method is complicated and there are problems such as precious metal shedding and biosecurity, which need to be further studied.

3.2. Type II heterojunction

Heterojunctions are usually defined as an interface between two regions of different semiconductors with different band

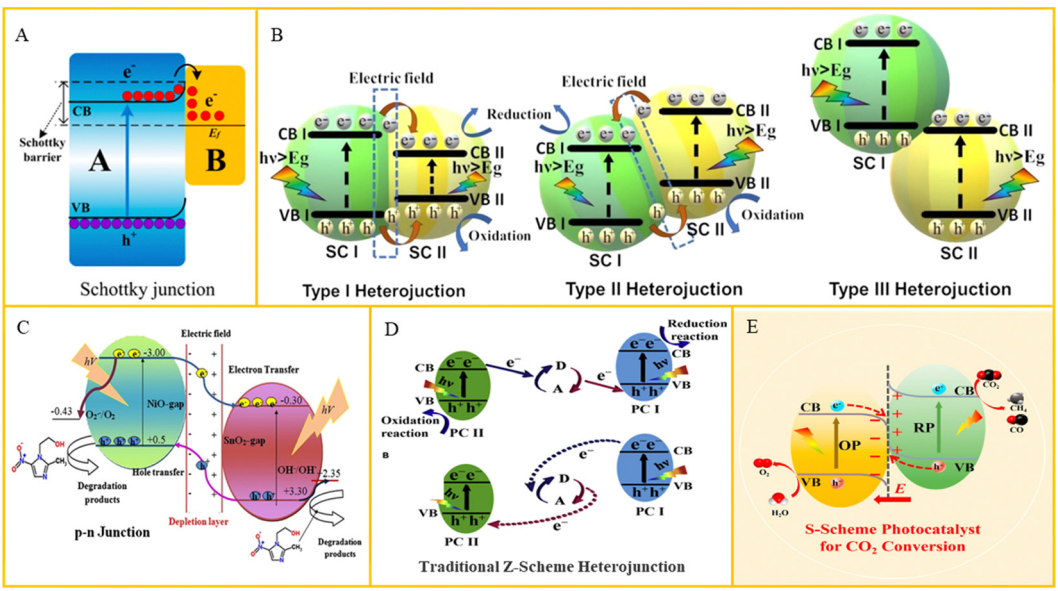

Fig. 3 (A) Schematic of charge transfer in the Schottky junction. Reproduced with permission.[88] Copyright 2020, MDPI. (B) Schematic of charge distribution in type I, type II and type III heterojunctions. Reproduced with permission.[89] Copyright 2023, Elsevier. (C) Schematic of carrier production and charge separation in an NiO–SnO_2 system. Reproduced with permission.[90] Copyright 2017, Elsevier. (D) Charge transfer route in a traditional Z-scheme heterojunction. Reproduced with permission.[91] Copyright 2020, Elsevier. (E) Schematic of the charge transfer route in an S-scheme heterojunction. Reproduced with permission.[92] Copyright 2023, Elsevier.

structures, and they can produce an interfacial band arrangement. According to the difference in the CB and VB energy levels of two semiconductors, the heterojunction formed can be divided into three types, namely, type I (transversal gap), type II (staggered gap) and Type III (broken gap), as shown in Fig. 3(B). For the type II heterojunction, both the VB and CB of semiconductor A are higher than that of semiconductor B. As a result, the photogenerated carriers can be separated because the excited electrons will be easily transferred. Yang *et al.*[93] constructed a core–shell interface electric field at the interface between metal organic framework (MOF) and two-dimensional MoS_2 nanosheets by *in situ* growth of MoS_2 on the surface of MOF, which it exhibited an antimicrobial efficiency of 99.73% and 99.58% against *S. aureus* and *E. coli* within 20 min. The problem of the type II heterojunction photocatalyst is that the redox reaction is carried out on the semiconductor with low redox potential, which inhibits its redox ability. At the same time, the electrostatic repulsion of electrons and holes also prevents their migration between semiconductors.

3.3. P–N heterojunction

P–N heterojunction is constructed with a P type heterojunction and an N type heterojunction, where the generation of additional electric fields at the interface can improve the electrons transfer (Fig. 3(C)). Li *et al.*[94] prepared Cu_2O–TiO_2 photocatalytic composites with the homogeneous distribution of P–N heterostructures by supercritical solvothermal method. Holes were the main active substances that reduced water to $^{\bullet}OH$, while the Cu_2O–TiO_2 interaction caused K^+ leakage. The antibacterial effect of several common pathogens, such as *Pseudomonas aeruginosa*, *E. coli* and *S. aureus*, was almost 100%. Ma *et al.*[95] prepared $Cu_{1.96}S$/g-MnO_2 P–N heterojunction, and the photoluminescence strength of $Cu_{1.96}S$/g-MnO_2 nanocomposites was low, which further indicated that P–N heterojunction significantly inhibited the recombination of charge pairs. However, P–N heterojunction is prone to photoinactivation under light irradiation, especially in an oxidizing environment, such as oxygen in the air, which will induce the oxidation of the heterojunction surface, resulting in reduced catalytic activity.

3.4. Type Z heterojunction

The above heterojunctions have the problem that the redox reaction is carried out on the semiconductor with low redox potential. Type Z photocatalysts can be divided into indirect type Z and direct type Z (type S) photocatalysts. The indirect Z heterojunction consists of two photocatalyst semiconductors and an intermediate A/D. Under photoexcitation, the intermediate A/D causes electrons to transfer indirectly from the CB of one semiconductor to the VB of another. Specifically, the photoelectrons reduce A to D, and subsequent holes oxidize D to A (Fig. 3(D)). The electrons are concentrated in semiconductor I and the holes are concentrated in semiconductor I, both of which have good redox ability. This system inhibits the recombination of electrons and holes, improves the redox capacity, and sacrifices part of the carrier to promote charge separation.[96] For direct type Z photocatalysts, two different semiconductors without the intermediate are needed, as shown in Fig. 3(E). The photogenerated electrons migrate directly from the CB of one semiconductor to the VB of another, leaving electrons and holes at a high redox potential.[97] Zhao *et al.*[98] prepared an organic–inorganic S-scheme heterojunction by carboxyl-modified polythiophene-based linear conjugated polymer and TiO_2, where under white light irradiation for 20 min, the heterojunction materials showed significant antibacterial properties, killing 3.86×10^7 cfu mL^{-1} MRSA. Jiang *et al.*[99] developed a Z-scheme heterojunction composed of single Ag atoms-anchored polymeric carbon nitride (Ag–PCN) and SnO_{2-x}, where the synergy between the single Ag atoms and the Z-scheme heterojunction initiated a cascade electron transfer from SnO_{2-x} to Ag–PCN and then to O_2 adsorbed on Ag. A type Z photocatalytic system can not only reduce electron–hole recombination but also maintain excellent redox ability. However, most synthetic artificial type Z photocatalytic systems usually have precious metals or redox pairs, which will bring great difficulties to their practical application.

4. Expansion of light response range

In addition to the problem of photogenerated electron and hole recombination, the semiconductor photocatalyst also have the problem of low light utilization. Most semiconductor photocatalysts have a wide band gap and can only absorb UV light and some visible light, but UV light only accounts for a small part of the sunlight. Therefore, it is very important to enlarge the light absorption range of semiconductor photocatalysts. This paper mainly introduces the methods to expand the light response range of semiconductor photocatalysts, including element doping, sensitization and up-conversion luminescence.

4.1. Element doping

Element doping can change the band structure of a semiconductor and generate visible light excitation and photoelectron transition. The doping of elements will affect the outermost orbital of the semiconductor, and metal ions or non-metal ions can enter the band gap as an intermediate stage. Also, the variant phase will narrow the band gap and cause the redshift of the absorption wavelength, further expanding the light wave response range and generating visible light response. On the other hand, the doping of elements causes the covalent bond between the atoms inside the semiconductor to break, resulting in certain defects in the crystal and formation of oxygen vacancies. A low concentration of oxygen vacancies can strengthen the transport of carriers and capture of photoelectrons, inhibit electron–hole recombination, and increase the visible light response. At present, element doping mainly includes metal and non-metal element doping. Metals have semiconductor-like properties, and their addition can strengthen the band gap structure of the semiconductor (Fig. 4(A)), increase the oxygen vacancy, which acts as an electron trap, and help to enhance the charge separation of photoactivity, thus improving the photocatalytic efficiency.[100]

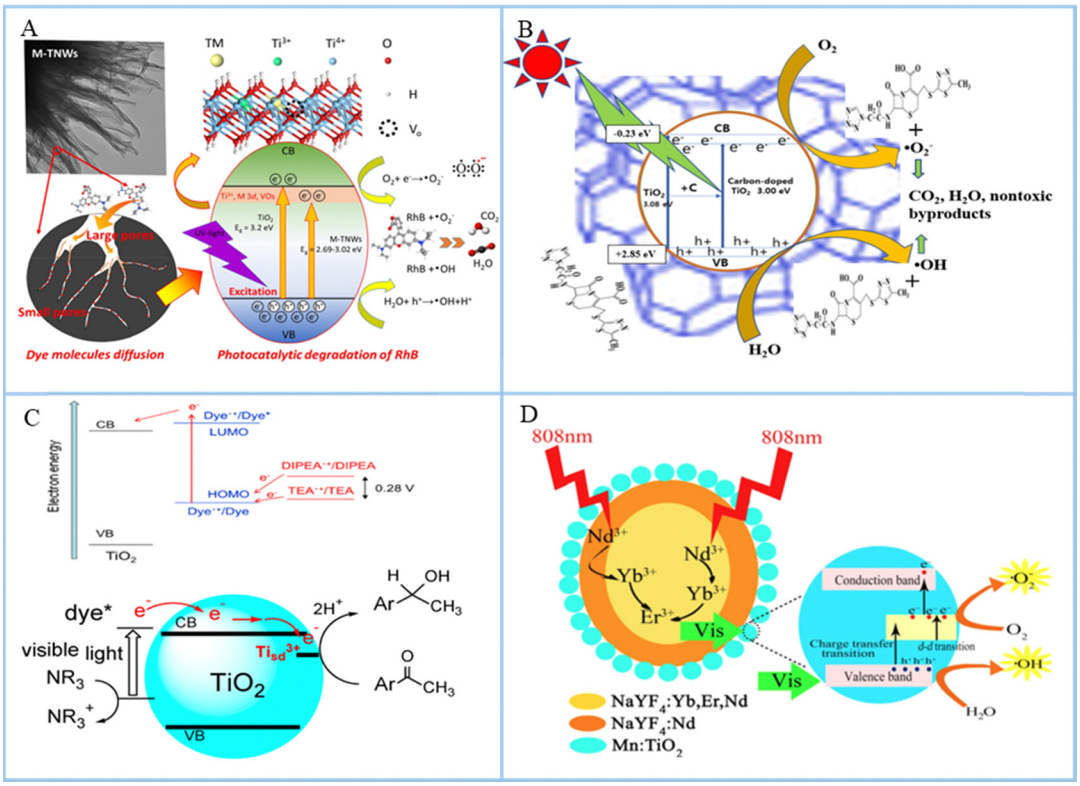

Fig. 4 (A) Schematic of the proposed reaction mechanisms of the photocatalytic degradation of RhB by transition-metal doped titanate nanowire photocatalysts. Reproduced with permission.[102] Copyright 2022, Elsevier. (B) Mechanisms of pollutant degradation using a zeolite carbon-doped TiO_2 nanocomposite under sunlight. Reproduced with permission.[103] Copyright 2023, Springer Nature. (C) Energetics and electron transfer processes and degradation of acetophenone derivatives occurring on dye-sensitized TiO_2. Reproduced with permission.[104] Copyright 2015, MDPI. (D) Schematic of the working mechanisms for the Yb/Er/Nd@Nd@Mn:TiO_2 photocatalyst under 808 nm NIR irradiation. Reproduced with permission.[105] Copyright 2019, American Chemical Society.

Although ion doping can improve the ROS production of semiconductors, the biocompatibility of metal ions needs to be further studied. Doped non-metallic elements can improve the relative stability of semiconductors with improved optical quantum efficiency due to their stable valence bond structure and unique charge distribution (Fig. 4(B)). Moreover, non-metallic doping can cause a redshift of optical absorption edge and show the effect of visible light absorption. Common doped non-metallic elements are N, C, F, B, and S.[101] However, the influence of specific gravity and doping amount of different nonmetallic elements on the visible light response range of semiconductors needs to be further confirmed.

4.2. Sensitization

The addition of sensitizers can broaden the semiconductor absorbance spectrum, which can produce a response to visible light or even NIR light. Sensitizers will be absorbed on the surface of TiO_2 with a narrow band gap and higher CB position than TiO_2. When photoexcited, optical quantum is absorbed to produce electronic transition, the chemical potential of the excited state is more negative than that of the CB, and the excited electron transfer is injected into the CB of TiO_2. The electrons in the CB will be transferred to the surface to participate in the photocatalytic reaction, thus expanding the wavelength response range of TiO_2 (Fig. 4(C)). Yang *et al.*[106] studied the design process of chlorophyll-sensitized TiO_2. They used a one-step synthesis method to extract chlorophyll from spinach and dope it into TiO_2 by heating the reactor. The results showed that TiO_2 doped with chlorophyll possessed two different absorption bands near 407 and 668 nm, indicating that the chlorophyll-sensitized TiO_2 had wide absorption from UV to visible light region. Wei *et al.*[107] synthesized CdSe quantum dot (QDs)-sensitized TiO_2 photoanode on fluorine-doped tin oxide-coated glass by molten salt-assisted self-assembly and constructed an efficient photoelectric chemical sensor to detect rutin. It was found that CdSe could transfer photoexcited electrons to the CB of TiO_2 and improve the photoelectric activity of TiO_2. In conclusion, the addition of sensitizer to TiO_2 could broaden the spectral range of TiO_2, generate visible light response, and improve the optical quantum efficiency. However, due to the different components and types of sensitizers and catalytic antibacterial materials, the mechanism of action in the process of photocatalytic antibacterial effect is more complicated and needs to be further studied.

4.3. Up-conversion luminescence

Many semiconductors cannot be excited by NIR light, and the UV light that excites them and part of the visible light used in bone tissue engineering can damage normal human tissue. In

Table 2 Application of semiconductor photocatalytic antibacterial materials in bone tissue engineering

Application	Materials	Bacteria or cells	Efficiency	Antibacterial substance	Function	Ref.
Osteosarcoma	TiO_2	*S. aureus*	98.7%	• NO • ROS	Ablate the tumor and eliminate the biofilm	109
Implant	S-TiO_2	*S. aureus*	99.995%	• PTT • ROS	Effective antibacterial activity and accelerated bone integration *in vivo*	110
Implant	TiO_2	MRSA	98%	• ROS	Prevents implant infection and promotes bone tissue regeneration	38
Dental implant	TiO_2	*Streptococcus sanguis*	—	• ROS	Reduce the biofilm on the surface of dental implants	111
Bone scaffold	ZnO	*E. coli*	99.9%	• ROS	Excellent photocatalytic antibacterial ability and good cytocompatibility for cell activity and proliferation	112
Implant	Bi_2S_3	*S. aureus*	99.45%	• Ag^+ • ROS	NIR light effectively eliminates biofilms in a short time	113
Osteosarcoma	TiO_2	Osteosarcoma cell	100%	• ROS • PTT	Ablating osteosarcoma and promoting osteogenic differentiation of cells	114
Osteosarcoma	ZnO	Osteosarcoma cell	48%	• Zn^{2+} • Fe^{3+} • ROS	Good antibacterial activity and good cytocompatibility	115
Osteomyelitis	MoS_2	MRSA	99.58%	• Zn^{2+} • ROS	Treat MRSA infection osteomyelitis and promote bone growth	116
Arthritis	CeO_2	Synovial cells	67.2%	• PTT • ROS	Synovial cell proliferation and gradual elimination of bone erosion	117
Osteomyelitis	MoS_2	*S. aureus*	—	• ROS	Treatment of osteomyelitis caused by *S. aureus*	118
Osteomyelitis	$BaTiO_3$	*S. aureus*	99%	• ROS	Removes pathogens and enhances osteoblast adhesion and differentiation	119
Bone scaffold	TiO_2	*S. aureus*	100%	• ROS	Enhanced mitochondrial activity and proliferation without inducing additional intracellular ROS of osteoblasts and promoted osseointegration in infected rat tibias	120
Periodontitis	Copper tannic acid coordination	*Porphyromonas gingivalis* *Actinomyces viscosus* *S. aureus* *E. coli*	98.51% 97.17% 93.13% 90.51%	• ROS	Antibacterial, antiplaque properties, and the expression of osteogenetic genes successively	121
Osteomyelitis	ZnO	*S. aureus* *E. coli*	74.18% 63.02%	• Zn^{2+} • ROS	Excellent antibacterial activity and enhanced bone regeneration	122
Dental implants	ZnO, TiO_2	Oral pathogens	75%	• Zn^{2+} • ROS	Higher capability for enhancing bone regeneration, antibiosis, and osseointegration	123
Bone scaffold	TiO_2 MoS_2	*S. aureus*	75%	• ROS • PTT	Synergistic antibacterial effect of ROS and PTT	124
Implant	TiO_2	*E. coli* *S. aureus*	100% 99.9%	• ROS • PTT	Rapid bactericidal method with high biosafety based on multiple synergistic antimicrobial methods	82
Implant	TiO_2/GO	*Streptococcus mutans*	—	• ROS • PTT	Excellent antibacterial activity and minimal inflammatory response	125
Implant	Cus/GO	*S. aureus*	—	• ROS • PTT	Endowing powerful antibacterial and bone-promoting abilities for implant-associated infections	126
Bone scaffold	ZnO	*E. coli* *S. aureus*	87.0% 88.4%	• Zn^{2+} • ROS	High cell compatibility and antimicrobial rate	127

addition, their penetration is not as good as NIR light and cannot reach the inside of bone tissue. Up-conversion materials are those with anti-Stokes properties, which can convert infrared light to shorter wavelengths of light (Fig. 4(D)). The most widely used material with the highest light conversion efficiency is $NaYF_4$. Zhang *et al.*[108] synthesized an up-conversion photocatalytic system (UCNPs-CPZ-PVP) using a β-carboxylic phthalocyanine (CPZ) molecule, up-conversion nanoparticles ($LiYF_4$:Yb/Er) and polyethylpyrrolidone (PVP). The UCNPs-CPZ-PVP could absorb NIR and release ROS, and it had good bacteriostatic effect on *S. aureus* and *E. coli*. However, photoconversion materials are often difficult to biodegrade, which hinders their application in bone tissue engineering.

5. Application in bone tissue engineering

Semiconductor photocatalytic antibacterial materials have been used in bone tissue engineering, including osteomyelitis treatment, bone defect repair and dental tissue regeneration. Some examples of the application in bone tissue engineering are shown in Table 2.

5.1. Osteomyelitis treatment

Bacterial infection due to trauma or surgery is a major cause of osteomyelitis, and severe osteomyelitis can lead to osteoporosis and pathological fractures. At present, the clinical treatment of osteomyelitis mainly relies on anti-infective drugs and surgical intervention, but drug therapy takes many weeks and is prone to relapse, while surgical debridement may aggravate bone loss. Semiconductor photocatalysis technology provides a new strategy for the treatment of osteomyelitis, such as the use of ROS produced by photocatalysis to inhibit bacterial growth; some examples are shown in Fig. 5. Li *et al.*[128] prepared Zn-doped C_3N_4 by two high-temperature combustion processes aimed at osteomyelitis caused by bacterial infection. The results demonstrated that after secondary calcination, the incorporation of Zn^{2+} into C_3N_4 improved its electronic structure and promoted interfacial polarization and electron transfer. Under microwave irradiation, the resulting plasma collided with oxygen, producing $^1O_2$ and $^\bullet O_2^-$, and the eradication rate of *S. aureus* reached 99.8% within 15 min. In addition, the released Zn^{2+} promoted the polarization of macrophages, further enhancing bone repair.

Jin *et al.*[130] used MoS_2/Fe_3O_4 to treat *S. aureus* infectious osteomyelitis. The experimental results indicated that the magnetic coordination between ROS produced by MoS_2/Fe_3O_4 and Fe_3O_4 increased the thermal sensitivity and permeability of bacterial cell membrane, prevented bacteria from spreading through the blood, targeted bacteria and killed them *in situ*. Wu *et al.*[129] prepared core–shell heterojunction ZnO/Ag_2S nanoparticles by a wet chemical method for the treatment of early

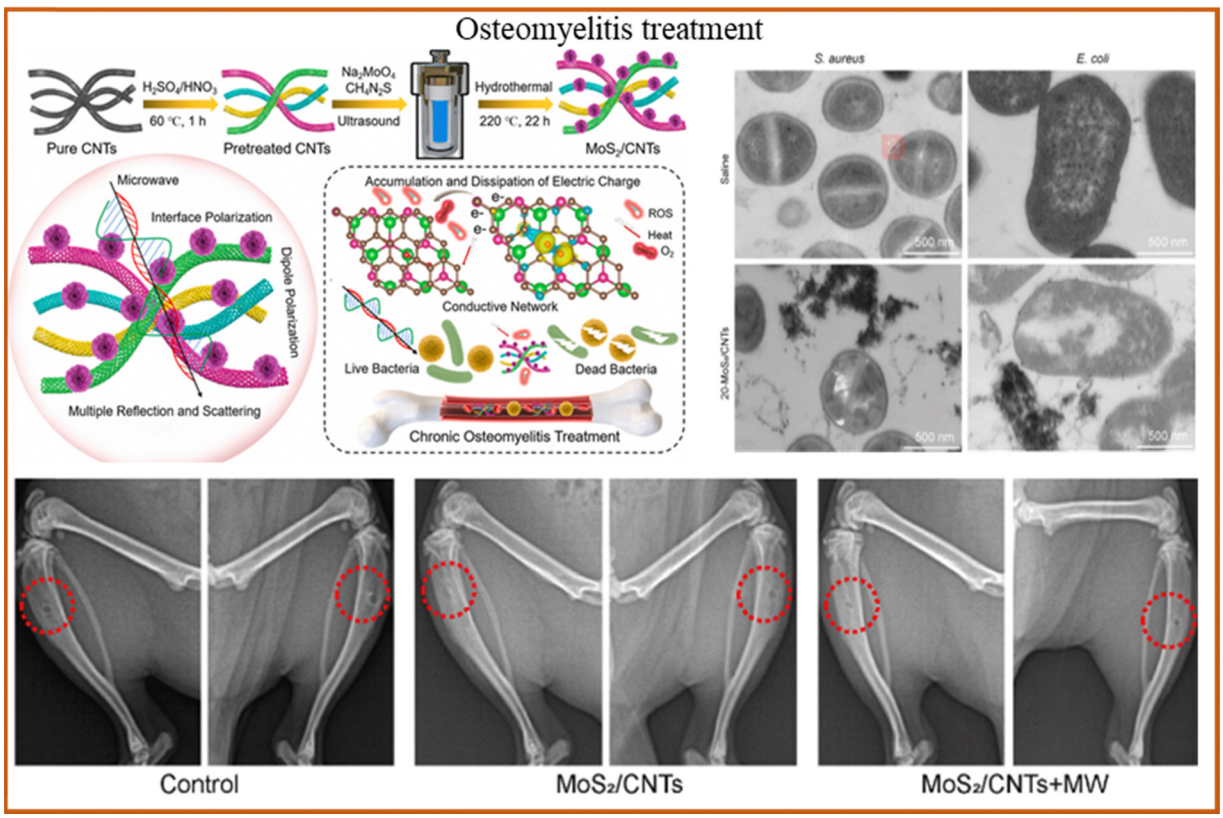

Fig. 5 MoS_2/CNTs heterojunctions generate heat and ROS under light, enabling treatment of deep tissue infections. TEM images of *S. aureus* and *E. coli* co-culture samples, and X-ray images of the tibias of the mice. Reproduced with permission.[129] Copyright 2024, Elsevier.

bacterial infection in osteomyelitis. The experimental results showed that 99.9% of *E. coli* and *S. aureus* could be eradicated after 10 min of irradiation when the material concentration was 100 μg mL^{-1}. In addition, the release of Zn ions showed good osteogenic effect. However, existing research shows that the recurrence rate of osteomyelitis is still high, most treatment methods are still in the experimental stage, and few have been applied in clinical practice. In the future, the targeted treatment strategy of minimally invasive injection may be an important development direction of osteomyelitis treatment.

5.2. Bone defect repair

Bone scaffold is an effective means to treat bone defect, but it can easily lead to implant-related infection during implantation, resulting in implantation failure and secondary damage to patients.[131–144] Therefore, improving the antimicrobial performance of bone scaffold is an effective strategy to deal with implant infection. For example, the antibacterial effect of bone scaffold is enhanced by introducing antibacterial components or surface modifications into the material (Fig. 6). Ullah *et al.*[145] indicated that Ca and P-doped ZnO nanorods were grown on Ti implant by hydrothermal method to deal with the antibacterial effect of the implant and promote the balance between bones. The results showed that the samples exhibited excellent antibacterial effects against *E. coli* and *S. aureus* and improved the inflammatory response around the implant.

Wang *et al.*[38] synthesized graphitic acetylene/TiO_2 nanofibers by electrostatic assembly to prevent implant bacterial infection. The nanofibers displayed excellent photocatalytic properties and produced a large amount of ROS, which induced bacterial cell wall perforation, cell membrane leakage, and eventually bacterial death. The antibacterial experiment indicated that the antibacterial rate of nanofibers against MRSA reached 98%. In addition, the results of the section of the femur tissue indicated that the nanofiber group had a higher antibacterial effect and bone-inducing ability than the other groups. Lu *et al.*[148] prepared chitosan nanofiber membrane modified with fucoidan and CuS for the prevention of bone infection. The results showed that the antibacterial activity of nanofibers against *S. aureus* and *E. coli* reached 99% under

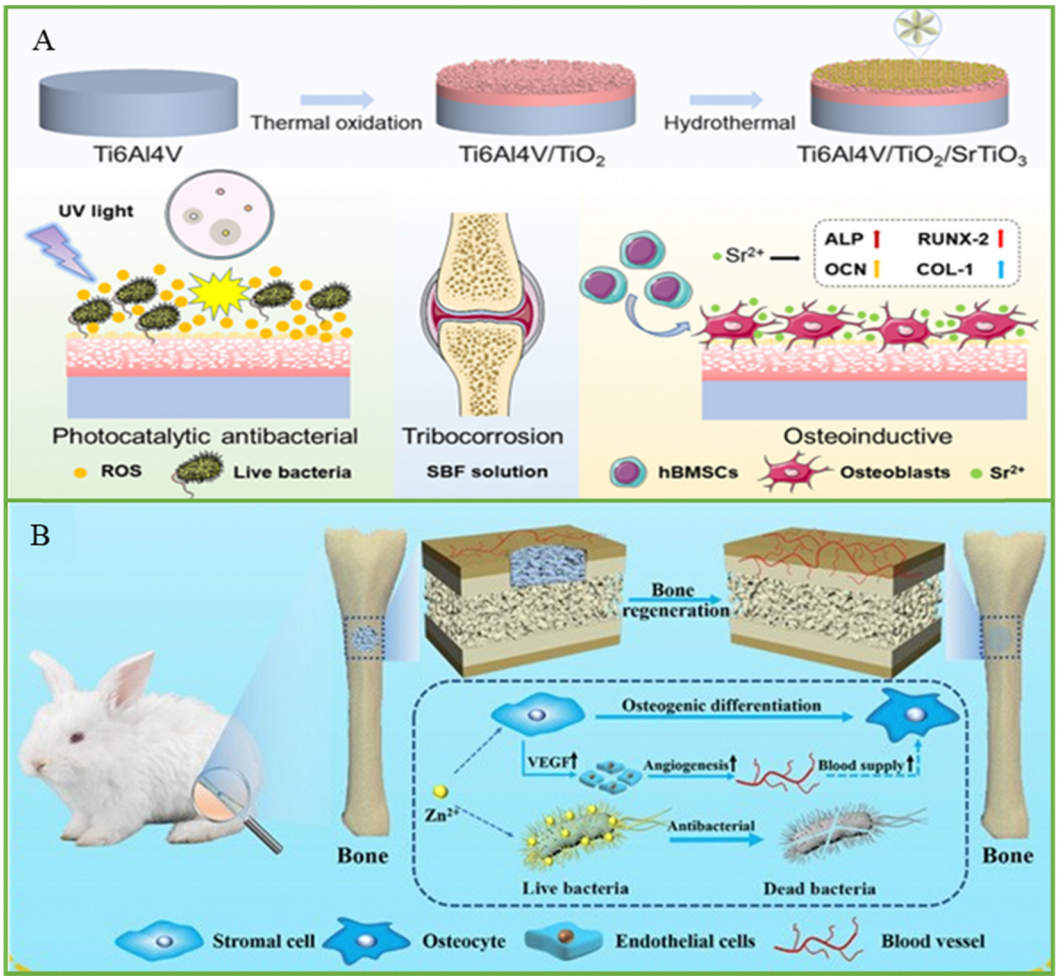

Fig. 6 (A) Schematic of the $TiO_2/SrTiO_3$ coating with photocatalytic antibacterial and osteogenesis properties, and the colony of *E. coli* on a plate after incubating with different samples under dark and UV light. Reproduced with permission.[146] Copyright 2022, Elsevier. (B) Schematic of a bone implant with antibacterial and accelerated bone reconstruction functions. Reproduced with permission.[147] Copyright 2023, Springer Nature.

light and had good biocompatibility. At present, manufacturing technology has provided assistance for the development of bone scaffolds,[149–155] but the antibacterial research on bone scaffolds is still mainly in the theoretical and experimental stages, and the intensity damage of scaffolds and potential damage to human body caused by the light required for photocatalytic antibacterial treatment need to be further evaluated.

5.3. Dental tissue regeneration

Tooth loss due to aging, periodontitis, dental caries and other factors seriously affect people's quality of life. Thus, dental implantation becomes an effective means to solve this problem. However, dental implantation surgery is prone to contact with a variety of bacteria, which can adhere to the surface of the implant, causing peri-implant inflammation. Currently, most dental implants are made of ceramic or metal materials such as Ti and its alloys, zirconia, but these materials do not have antibacterial properties on their own. In order to improve the antimicrobial properties of dental implants, researchers have made many explorations (Fig. 7). For example, the production of a TiO_2 oxide layer on the surface of Ti implant by anodization is considered to be an effective way to deal with peri-implant inflammation. Heloisa *et al.*[156] developed TiO_2 films with different crystal phases by magnetron sputtering deposition, which showed good antibacterial activity on oral multi-species biofilm models. It is a technology that has the potential to reduce biofilms on the surface of implant abutment, and its photocatalytic effect plays a positive role in the treatment of oral biofilm-related diseases.

Chen *et al.*[158] designed ZnO/TiO_2 heterojunction nanofilms with photoresponsive properties on the surface of Ti implant to solve the problem of insufficient anti-infection ability of implanted teeth. The nanothin films enhanced the photothermal and photoelectric properties of the implant under NIR irradiation by reducing the band gap and improving the interfacial charge transfer efficiency. Experiments indicated that the implant exhibited excellent broad-spectrum antibacterial effect against three dental pathogens (*Porphyromonas gingivalis*, *Clostridium nucleatum* and *S. aureus*) by destroying the bacterial membrane and increasing the production of intracellular ROS with a bactericidal rate of more than 99.4%. However, the antibacterial strategy of dental implants has not been widely used in clinical practice, and the artificial antibacterial model cannot fully reproduce the complex environment of human implants. Meanwhile, the biocompatibility of antibacterial materials still needs to be further verified. The future direction of development is to develop materials that meet the

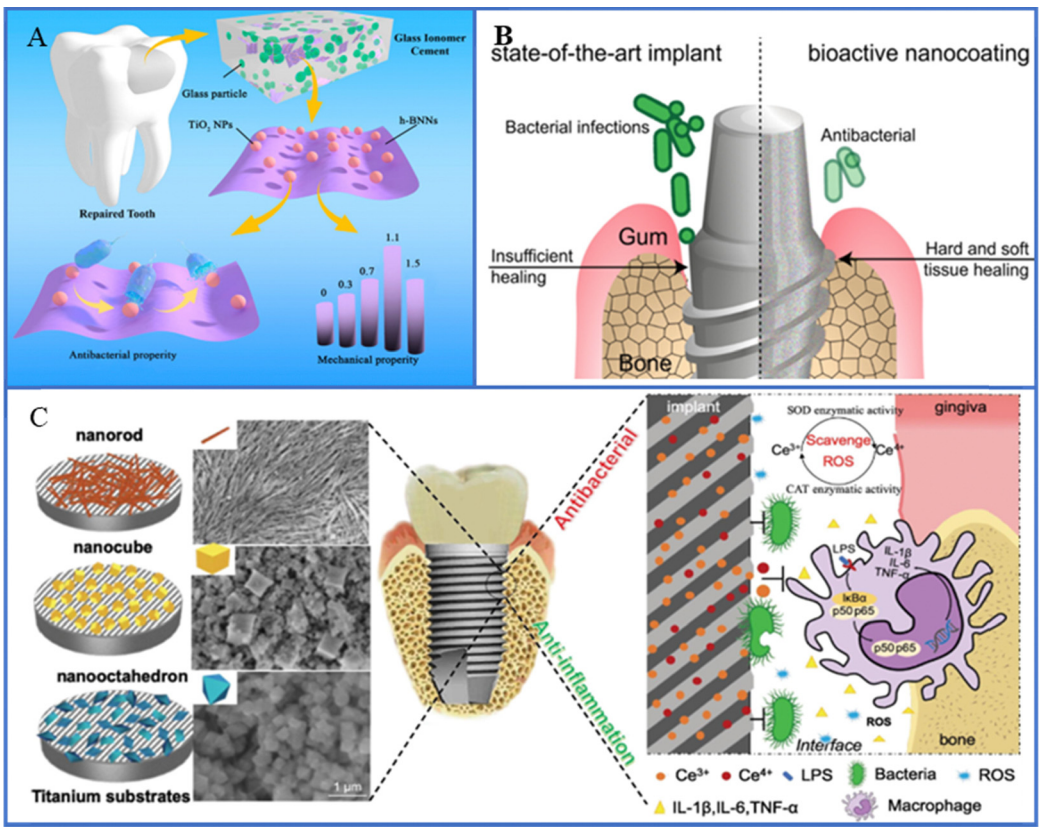

Fig. 7 (A) Schematic of synthesis and performance evaluation of hexagonal boron nitride nanosheet/TiO_2 composites. Reproduced with permission.[157] Copyright 2022, Frontiers Media. (B) Schematic diagram of versatile antimicrobial nano-architected implant coatings for hard and soft tissue healing. Reproduced with permission.[18] Copyright 2021, American Chemical Society. (C) Schematic illustration of implant surface modified by nano-CeO_2 for antibacterial and anti-inflammatory properties. Reproduced with permission. Copyright 2019, Elsevier.

requirements of dental implant with antibacterial function, facilitate the integration of the implant with the surrounding tissue, and provide personalized solutions for different patients.

6. Conclusions and future prospects

This article summarized the semiconductor materials used for photocatalytic antibacterial treatment, the strategies for improving photocatalytic properties, and their applications in bone tissue engineering. According to the difference in their carriers, semiconductors can be divided into P-type and N-type, and several commonly used photocatalytic semiconductor materials are introduced, such as TiO_2, ZnO, and g-C_3N_4. In order to further improve the antibacterial effect, the efficiency of photocatalysis is improved by reducing the recombination of carriers and expanding the photoresponse range, and the specific methods are summarized such as construction of heterojunction, element doping, and up-conversion luminescence. Finally, the research on the application of semiconductor photocatalytic antimicrobial treatment in bone tissue engineering is summarized, including osteomyelitis treatment, bone defect repair and dental tissue regeneration.

Although semiconductor photocatalytic materials have been used to combat bacterial infection in bone tissue engineering, their clinical applications are still limited, mainly due to the following unresolved issues. Firstly, the biocompatibility of the material is key, but the ROS produced by photocatalysis may damage normal cells, which is not conducive to bone repair, and the clearance of nanomaterials *in vivo* is also an obstacle.[159] Secondly, the lack of standardized models to evaluate the effectiveness of these materials, especially antimicrobial properties and long-term properties, makes comparisons with different bacteria and conditions difficult.[160] Thirdly, cumbersome regulatory requirements further complicate the journey from lab to market. To achieve efficient clinical translation, academia, industry and regulators need to work closely together. In recent years, photocatalytic therapy has been transformed into a synergistic therapy by combining with other antimicrobial approaches, bringing the expected benefits, but increasing the composition adjustment and pharmacological complexity, which in turn increases the difficulty of approval.[159–162] To overcome these challenges, technologies such as materials genomics, artificial intelligence and machine learning can help drive development, while interdisciplinary collaboration is also key to accelerating the transformation of antimicrobial phototherapy. Semiconductor photocatalytic antimicrobial technology has great potential in the field of bone repair from basic research to clinical application, and future research should focus on the design of multi-functional semiconductor materials with both efficient photocatalytic performance and excellent biocompatibility to meet the needs of bone repair. In addition, research on bone repair and implants should focus on how to design semiconductor materials with durable antibacterial properties and avoid toxic effects on host cells. Through these technological breakthroughs, semiconductor photocatalytic antimicrobial technology can play an important role in the field of bone repair, promoting its transformation from laboratory research to clinical application.

Data availability

Raw data are available from the corresponding author upon reasonable request.

Conflicts of interest

There are no conflicts to declare.

Acknowledgements

This work was supported by the following funds: (1) The Natural Science Foundation of China (52275393, 52475362); (2) National Key Research and Development Program of China (grant no. 2023YFB4605800); (3) Jiangxi Provincial Natural Science Foundation of China (20224ACB204013); (4) The Project of State Key Laboratory of Precision Manufacturing for Extreme Service Performance; (5) Natural Science Foundation of Hunan Province (2023JJ30461); (6) The Science Foundation of Hunan University of Chinese Medicine (Z2023JBGS04); (7) The Fundamental Research Funds for the Central Universities of Central South University (2024ZZTS0325).

References

1 Y. Zhao, J. Li, L. Liu, Y. Wang, Y. Ju, C. Zeng, Z. Lu, D. Xie and J. Guo, *Adv. Healthcare Mater.*, 2023, **12**, 2300303.
2 D. Huo, F. Wang, F. Yang, T. Lin, Q. Zhong, S.-P. Deng, J. Zhang, S. Tan and L. Huang, *J. Mater. Sci. Technol.*, 2024, **179**, 208–223.
3 Z. Yu, Z. Wang, Y. Chen, Y. Wang, L. Tang, Y. Xi, K. Lai, Q. Zhang, S. Li, D. Xu, A. Tian, M. Wu, Y. Wang, G. Yang, C. Gao and T. Huang, *Biomaterials*, 2025, **313**, 122772.
4 B. Fang, P. Qiu, C. Xia, D. Cai, C. Zhao, Y. Chen, H. Wang, S. Liu, H. Cheng, Z. Tang, B. Wang, S. Fan and X. Lin, *Biomaterials*, 2021, **268**, 120603.
5 Y. Ren, J. Weeks, T. Xue, J. Rainbolt, K. L. de Mesy Bentley, Y. Shu, Y. Liu, E. Masters, P. Cherian, C. E. McKenna, J. Neighbors, F. H. Ebetino, E. M. Schwarz, S. Sun and C. Xie, *Bone Res.*, 2023, **11**, 51.
6 S. Huo, Z. Lyu, X. Su, F. Wang, J. Liu, S. Liu, X. Liu, X. Bao, J. Zhang, K. Zheng and G. Xu, *Composites, Part B*, 2023, **253**, 110521.
7 X. Zhang, Q. Li, L. Li, J. Ouyang, T. Wang, J. Chen, X. Hu, Y. Ao, D. Qin, L. Zhang, J. Xue, J. Cheng and W. Tao, *ACS Nano*, 2023, **17**, 6466–6479.
8 D. Mo, M. Pan, W. Chen, Q. Liu, Y. Yu, L. Yuan, Y. Yang, H. Deng, M. Wang and Z. Qian, *Adv. Funct. Mater.*, 2024, **34**, 2313569.

9 L. Zhou, Y. Deng, Y. Ren, H. L. Poon, W. Y. Chu, H. Wang and Y. K. Chan, *Chem. Eng. J.*, 2024, **482**, 148978.
10 Q. Yu, C. Wang, X. Zhang, H. Chen, M. X. Wu and M. Lu, *ACS Nano*, 2024, **18**, 14085–14122.
11 X. Wang, X. Wan, X. Qin, C. Chen, X. Qian, Y. Guo, Q. Xu, W.-B. Cai, H. Yang and K. Jiang, *ACS Catal.*, 2022, **12**, 9437–9445.
12 Y. Liu, M. Wang, B. Zhang, D. Yan and X. Xiang, *ACS Catal.*, 2022, **12**, 6946–6957.
13 Z. Zhang, J. Fan, J. Du and X. Peng, *Coord. Chem. Rev.*, 2021, **427**, 213575.
14 F. Dalanta, T. D. Kusworo and N. Aryanti, *Appl. Catal., B*, 2022, **316**, 121576.
15 A. Ali, J. Lee, K. Kim, H. Oh and G.-C. Yi, *Adv. Healthcare Mater.*, 2024, **13**, 2304140.
16 U. M. Dankawu, H. Y. Hafeez, C. E. Ndikilar, J. Mohammed, A. B. Suleiman and A. S. Shuaibu, *Int. J. Hydrogen Energy*, 2024, **67**, 1218–1242.
17 T. O. Ajiboye and D. C. Onwudiwe, *Results Chem.*, 2021, **3**, 100151.
18 M. T. Matter, L. Maliqi, K. Keevend, S. Guimond, J. Ng, E. Armagan, M. Rottmar and I. K. Herrmann, *ACS Appl. Mater. Interfaces*, 2021, **13**, 33300–33310.
19 J. Murillo-Sierra, A. Hernández-Ramírez, L. Hinojosa-Reyes and J. Guzmán-Mar, *Chem. Eng. J. Adv.*, 2021, **5**, 100070.
20 P. Shandilya, S. Sambyal, R. Sharma, P. Mandyal and B. Fang, *J. Hazard. Mater.*, 2022, **428**, 128218.
21 Z. Thiehmed, A. Shakoor and T. Altahtamouni, *Catalysts*, 2021, **11**, 1283.
22 H. Moon, M. S. Goh, M. Cha, U.-S. Kim, H. S. Whang, N. Son and M. Kang, *Appl. Surf. Sci.*, 2022, **606**, 154787.
23 Z. Meng, J. Zhang, C. Jiang, C. Trapalis, L. Zhang and J. Yu, *Small*, 2024, **20**, 2308952.
24 K. Sharma, S. Patial, P. Singh, A. A. P. Khan, V. Saini, A. K. Nadda, C. M. Hussain, V.-H. Nguyen, C. C. Nguyen and T. B. H. Nguyen, *Sol. Energy*, 2022, **231**, 546–565.
25 J.-C. Kao, J.-P. Chou, P.-J. Chen and Y.-C. Lo, *Mater. Today Phys.*, 2023, **38**, 101218.
26 P. Raizada, A. Sudhaik, S. Patial, V. Hasija, A. A. P. Khan, P. Singh, S. Gautam, M. Kaur and V.-H. Nguyen, *Arabian J. Chem.*, 2020, **13**, 8424–8457.
27 L. Isac, C. Cazan, L. Andronic and A. Enesca, *Catalysts*, 2022, **12**, 1135.
28 Y. Jing, K. Liang, N. S. Muir, H. Zhou, Z. Li, J. M. Palasz, J. Sorbie, C. Wang, S. K. Cushing, C. P. Kubiak, Z. Sofer, S. Li and W. Xiong, *Angew. Chem., Int. Ed.*, 2024, **63**, e202405123.
29 Y. Zi, J. Zhu, L. Hu, M. Wang and W. Huang, *Small. Sci.*, 2022, **2**, 2100098.
30 L. Che, J. Pan, K. Cai, Y. Cong and S.-W. Lv, *Sep. Purif. Technol.*, 2023, **315**, 123708.
31 Y. Duan, X. Zhu, Q. Luo, L. Wang, Z. Li and D. Wang, *J. Catal.*, 2021, **400**, 160–165.
32 M. Amarnath and K. Gurunathan, *J. Alloys Compd.*, 2021, **857**, 157584.
33 Z. Lin, C. Du, B. Yan and G. Yang, *J. Catal.*, 2019, **372**, 299–310.
34 J. Chu, G. Sun, X. Han, X. Chen, J. Wang, W. Hu, I. Waluyo, A. Hunt, Y. Du, B. Song and P. Xu, *Nanoscale*, 2019, **11**, 15633–15640.
35 S. Zhu, W. Liao, M. Zhang and S. Liang, *Chem. Eng. J.*, 2019, **361**, 461–469.
36 H. Sun, X. Guo and A. Facchetti, *Chem*, 2020, **6**, 1310–1326.
37 D. Yuan, W. Liu and X. Zhu, *Chem. Soc. Rev.*, 2023, **52**, 3842–3872.
38 R. Wang, M. Shi, F. Xu, Y. Qiu, P. Zhang, K. Shen, Q. Zhao, J. Yu and Y. Zhang, *Nat. Commun.*, 2020, **11**, 4465.
39 H. Mohd Yusof, R. Mohamad, U. H. Zaidan and N. A. Abdul Rahman, *J. Anim. Sci. Biotechnol.*, 2019, **10**, 57.
40 Z. Teng, N. Yang, H. Lv, S. Wang, M. Hu, C. Wang, D. Wang and G. Wang, *Chem*, 2019, **5**, 664–680.
41 Z. Xu, J. Wu, B. Lovely, Y. Li, M. Ponder, K. Waterman, Y.-T. Kim, D. Shuai, Y. Yin and H. Huang, *J. Hazard. Mater.*, 2024, **480**, 136296.
42 N. Thakur, N. Thakur, A. Kumar, V. K. Thakur, S. Kalia, V. Arya, A. Kumar, S. Kumar and G. Z. Kyzas, *Sci. Total Environ.*, 2024, **914**, 169815.
43 Y.-h Lyu, F. Wei, T. Zhang, L. Luo, Y. Pan, X. Yang, H. Yu and S. Zhou, *J. Alloys Compd.*, 2021, **876**, 160016.
44 C. Xiao, G. Dong, T. Liu, L. Wang and C. Zhu, *Sep. Purif. Technol.*, 2024, **347**, 127673.
45 S. Varnagiris, M. Urbonavicius, S. Sakalauskaite, R. Daugelavicius, L. Pranevicius, M. Lelis and D. Milcius, *Sci. Total Environ.*, 2020, **720**, 137600.
46 R. Wang, R. Liu, S. Luo, J. Wu, D. Zhang, T. Yue, J. Sun, C. Zhang, L. Zhu and J. Wang, *Chem. Eng. J.*, 2021, **421**, 129596.
47 J. Wang, Z. Wang, W. Wang, Y. Wang, X. Hu, J. Liu, X. Gong, W. Miao, L. Ding and X. Li, *Nanoscale*, 2022, **14**, 6709–6734.
48 R. C. Nonato, L. H. Mei, B. C. Bonse, C. V. Leal, C. E. Levy, F. A. Oliveira, C. Delarmelina, M. C. Duarte and A. R. Morales, *Polym. Eng. Sci.*, 2022, **62**, 1147–1155.
49 N. Babayevska, Ł. Przysiecka, I. Iatsunskyi, G. Nowaczyk, M. Jarek, E. Janiszewska and S. Jurga, *Sci. Rep.*, 2022, **12**, 8148.
50 W.-N. Wang, P. Pei, Z.-Y. Chu, B.-J. Chen, H.-S. Qian, Z.-B. Zha, W. Zhou, T. Liu, M. Shao and H. Wang, *Chem. Eng. J.*, 2020, **397**, 125488.
51 J. Guo, J. Zhou, Z. Sun, M. Wang, X. Zou, H. Mao and F. Yan, *Acta Biomater.*, 2022, **146**, 370–384.
52 R. Sakthivel, S. Kubendhiran and S.-M. Chen, *Ultrason. Sonochem.*, 2019, **54**, 68–78.
53 W.-N. Wang, C.-Y. Zhang, M.-F. Zhang, P. Pei, W. Zhou, Z.-B. Zha, M. Shao and H.-S. Qian, *Chem. Eng. J.*, 2020, **381**, 122630.
54 S. Puebla, R. D'Agosta, G. Sanchez-Santolino, R. Frisenda, C. Munuera and A. Castellanos-Gomez, *npj 2D Mater. Appl.*, 2021, **5**, 37.
55 Q. Gao, Z. Wang, Y. Rao, Y. Zhao, J. Cao, K.-F. Ho, Y. Zhai, M. Xiong, J. Li and Y. Huang, *J. Hazard. Mater.*, 2023, **443**, 130275.

56 Y.-Y. Yang, H.-P. Feng, C.-G. Niu, D.-W. Huang, H. Guo, C. Liang, H.-Y. Liu, S. Chen, N. Tang and L. Li, *Chem. Eng. J.*, 2021, **426**, 131902.
57 H. Boumeriame, E. S. Da Silva, A. S. Cherevan, T. Chafik, J. L. Faria and D. Eder, *J. Energy Chem.*, 2022, **64**, 406–431.
58 T. S. Rad, Z. Ansarian, R. D. C. Soltani, A. Khataee, Y. Orooji and F. Vafaei, *J. Hazard. Mater.*, 2020, **399**, 123062.
59 E. Nikoomanzari and A. Fattah-alhosseini, *J. Magnesium Alloys*, 2024, **12**, 2674–2694.
60 D. Zhang, J. Zhou, F. Peng, J. Tan, X. Zhang, S. Qian, Y. Qiao, Y. Zhang and X. Liu, *J. Mater. Sci. Technol.*, 2022, **105**, 57–67.
61 Y. Xiong, D. Xu, Y. Feng, G. Zhang, P. Lin and X. Chen, *Adv. Mater.*, 2023, **35**, 2206939.
62 W. Lu, T. Gu, X. Jing, Y. Zhu, L. Yu, S. Hou, T. Pang, N. Lu and Z. Zhang, *J. Alloys Compd.*, 2023, **968**, 171864.
63 J. Zeng, Z. Li, H. Jiang and X. Wang, *Mater. Horiz.*, 2021, **8**, 2964–3008.
64 H. Siddiqui, M. S. Qureshi and F. Z. Haque, *Nano-Micro Lett.*, 2020, **12**, 29.
65 J. Liu, B. Yin, S. Li, L. Mi, G. Yin, F. Li, L. Zhong, N. Bai and X. Li, *J. Ind. Eng. Chem.*, 2024, **133**, 345–354.
66 F. Chen, Y. Luo, X. Liu, Y. Zheng, Y. Han, D. Yang and S. Wu, *Adv. Healthcare Mater.*, 2022, **11**, 2200360.
67 H. Bahramian, A. Fattah-alhosseini, M. Karbasi, E. Nikoomanzari and S. Giannakis, *Chem. Eng. J.*, 2023, **476**, 146588.
68 G. Guan, L. Zhang, J. Zhu, H. Wu, W. Li and Q. Sun, *J. Hazard. Mater.*, 2021, **402**, 123542.
69 A. George, D. M. A. Raj, A. D. Raj, A. A. Irudayaraj, J. Arumugam, M. Senthil kumar, H. J. Prabu, S. J. Sundaram, N. A. Al-Dhabi, M. V. Arasu, M. Maaza and K. Kaviyarasu, *Surf. Interfaces*, 2020, **21**, 100761.
70 Z. Zou, J. Sun, Q. Li, Y. Pu, J. Liu, R. Sun, L. Wang and T. Jiang, *Colloids Surf., B*, 2020, **189**, 110875.
71 X. Xue, H. Zhang, H. Liu, S. Wang, J. Li, Q. Zhou, X. Chen, X. Ren, Y. Jing, Y. Deng, Z. Geng, X. Wang and J. Su, *Adv. Funct. Mater.*, 2022, **32**, 2202470.
72 X. L. Hu, L. Chu, X. Dong, G. R. Chen, T. Tang, D. Chen, X. P. He and H. Tian, *Adv. Funct. Mater.*, 2019, **29**, 1806986.
73 Z. H. Jabbar and B. H. Graimed, *J. Water Process Eng.*, 2022, **47**, 102671.
74 D. Shiny, D. Usha, P. M. Anjana, S. Smonia Joe Princy, M. H. Almutairi, B. O. Almutairi, M. R. Bindhu and T. M. Aminabhavi, *Chem. Eng. J.*, 2024, **498**, 155720.
75 R. Zhang, R. Chilivery, D. Yao, W. Chen, F. Lu, W. Gao, Y. Fang, Z. Zhong and Y. Song, *Appl. Surf. Sci.*, 2022, **574**, 151683.
76 S. Somekawa, H. Watanabe, Y. Ono, Y. Oaki and H. Imai, *Mater. Lett.*, 2021, **304**, 130609.
77 B. Sun, F. Wu, Q. Zhang, X. Chu, Z. Wang, X. Huang, J. Li, C. Yao, N. Zhou and J. Shen, *J. Colloid Interface Sci.*, 2021, **584**, 505–519.
78 C. Jing, Y. Zhang, J. Zheng, S. Ge, J. Lin, D. Pan, N. Naik and Z. Guo, *Particuology*, 2022, **69**, 111–122.
79 W. Wang, J. Fang and H. Chen, *J. Alloys Compd.*, 2020, **819**, 153064.
80 M. Kazemi, A. Akbari, Z. Sabouri, S. Soleimanpour, H. Zarrinfar, M. Khatami and M. Darroudi, *Bioprocess Biosyst. Eng.*, 2021, **44**, 1215–1225.
81 Y. Liu, Y. Tian, Q. Han, J. Yin, J. Zhang, Y. Yu, W. Yang and Y. Deng, *Chem. Eng. J.*, 2021, **410**, 128209.
82 X. Zhang, G. Zhang, M. Chai, X. Yao, W. Chen and P. K. Chu, *Bioact. Mater.*, 2021, **6**, 12–25.
83 M. Yang, S. Qiu, E. Coy, S. Li, K. Załęski, Y. Zhang, H. Pan and G. Wang, *Adv. Mater.*, 2022, **34**, 2106314.
84 F. Li, L. Cheng, J. Fan and Q. Xiang, *J. Chem. Mater. A*, 2021, **9**, 23765–23782.
85 J. Ma, T. J. Miao and J. Tang, *Chem. Soc. Rev.*, 2022, **51**, 5777–5794.
86 Y. Ma, D. Xu, W. Chen, Y. Tang, X. Wang, L. Li and J. Wang, *Appl. Surf. Sci.*, 2022, **572**, 151432.
87 M. Wang, L. Nian, Y. Cheng, B. Yuan, S. Cheng and C. Cao, *Chem. Eng. J.*, 2021, **426**, 130832.
88 J. Li, P. Jiménez-Calvo, E. Paineau and M. N. Ghazzal, *Catalysts*, 2020, **10**, 89.
89 D. Salazar-Marín, G. Oza, J. A. D. Real, A. Cervantes-Uribe, H. Pérez-Vidal, M. K. Kesarla, J. G. T. Torres and S. Godavarthi, *Appl. Surf. Sci. Adv.*, 2024, **19**, 100536.
90 H. Derikvandi and A. Nezamzadeh-Ejhieh, *J. Colloid Interface Sci.*, 2017, **490**, 314–327.
91 Q. Xu, L. Zhang, B. Cheng, J. Fan and J. Yu, *Chem*, 2020, **6**, 1543–1559.
92 A. Meng, B. Zhu, Y. Zhong, S. Zhou, P. Han and Y. Su, *Energy Rev.*, 2023, **2**, 100052.
93 Z. Yang, C. Chen, B. Li, Y. Zheng, X. Liu, J. Shen, Y. Zhang and S. Wu, *Chem. Eng. J.*, 2023, **451**, 139127.
94 H. Li, J. Zhong, H. Zhu, Y. Yang, M. Ding, L. Luo, Y. Huo and H. Li, *ACS Appl. Bio Mater.*, 2019, **2**, 4892–4903.
95 M. Faraji, N. Mohaghegh and A. Abedini, *J. Photochem. Photobiol., B*, 2018, **178**, 124–132.
96 Y. Lan, Z. Li, D. Li, W. Xie, G. Yan and S. Guo, *Chem. Eng. J.*, 2020, **392**, 123686.
97 F. Guo, W. Shi, M. Li, Y. Shi and H. Wen, *Sep. Purif. Technol.*, 2019, **210**, 608–615.
98 X. Zhao, S. Wang, D. Shan, Y. Xu, L. Wu, H. Guo, G. Che, C. Liu and J. Du, *Chem. Eng. J.*, 2024, **495**, 153675.
99 W. Jiang, H. Zhu, J. Yang, B. Q. L. Low, W.-Y. Wu, M. Chen, J. Ma, R. Long, J. Low, H. Zhu, J. Z. X. Heng, K. Y. Tang, C. H. T. Chai, M. Lin, Q. Zhu, Y.-W. Zhang, D. Chi, Z. Li, X. J. Loh, Y. Xiong and E. Ye, *Adv. Sci.*, 2023, **10**, 2303448.
100 E. Erusappan, S. Thiripuranthagan, R. Radhakrishnan, M. Durai, S. Kumaravel, T. Vembuli and N. J. Kaleekkal, *J. Environ. Chem. Eng.*, 2021, **9**, 105776.
101 S. Patnaik, D. P. Sahoo and K. Parida, *Carbon*, 2021, **172**, 682–711.
102 X. Lu, F. Liu, Y. Dang, M. Li, M. Ruan, M. Wu, C. Zhu, T. Mani, S. L. Suib and P.-X. Gao, *Appl. Surf. Sci.*, 2022, **591**, 153116.
103 M. S. Rajan, A. John, M. Yoon and J. Thomas, *Environ. Sci. Pollut. Res.*, 2023, **30**, 60638–60653.

104 S. Kohtani, M. Mori, E. Yoshioka and H. Miyabe, *Catalysts*, 2015, **5**, 1417–1424.
105 Z. Nie, X. Ke, D. Li, Y. Zhao, L. Zhu, R. Qiao and X. L. Zhang, *J. Phys. Chem. C*, 2019, **123**, 22959–22970.
106 H. Yang, Y. Yang, L. Jiang, Y. Wang, Y. Chen, J. He, W. Wang and J. Wang, *Nano Select*, 2022, **3**, 140–146.
107 L. Wei, X. Li and S. Feng, *Int. J. Electrochem. Sci.*, 2021, **16**, 151032.
108 Y. Zhang, P. Huang, D. Wang, J. Chen, W. Liu, P. Hu, M. Huang, X. Chen and Z. Chen, *Nanoscale*, 2018, **10**, 15485–15495.
109 G. Zhang, Z. Wu, Y. Yang, J. Shi, J. Lv, Y. Fang, Z. Shen, Z. Lv, P. Li, X. Yao, W. Chen, X. Wei, P. K. Chu and X. Zhang, *Chem. Eng. J.*, 2022, **428**, 131155.
110 K. Su, L. Tan, X. Liu, Z. Cui, Y. Zheng, B. Li, Y. Han, Z. Li, S. Zhu, Y. Liang, X. Feng, X. Wang and S. Wu, *ACS Nano*, 2020, **14**, 2077–2089.
111 B. E. Nagay, C. Dini, J. M. Cordeiro, A. P. Ricomini-Filho, E. D. De Avila, E. C. Rangel, N. C. Da Cruz and V. A. Barao, *ACS Appl. Mater. Interfaces*, 2019, **11**, 18186–18202.
112 C. Shuai, X. Yuan, Y. Shuai, G. Qian, J. Yao, W. Xu, S. Peng and W. Yang, *Mater. Today Nano*, 2022, **18**, 100210.
113 L. Hong, X. Liu, L. Tan, Z. Cui, X. Yang, Y. Liang, Z. Li, S. Zhu, Y. Zheng and K. W. K. Yeung, *Adv. Healthcare Mater.*, 2019, **8**, 1900835.
114 Z. Wu, Q. Tian, J. Wang, Y. Feng, L. Li, C. Xu, J. Lv and Z. Lv, *Colloids Surf., B*, 2022, **211**, 112296.
115 V. Saxena and L. M. Pandey, *J. Trace Elem. Med. Biol.*, 2020, **57**, 126416.
116 X. Feng, J. Lei, L. Ma, Q. Ouyang, Y. Zeng, H. Liang, C. Lei, G. Li, L. Tan, X. Liu and C. Yang, *Small*, 2022, **18**, 2105775.
117 Z. Li, X. Wu, W. Gu, P. Zhou, H. Chen, W. Wang, Z. Cai, S. Cao, K. Guo, X. Zheng and F. Gao, *Chem. Eng. J.*, 2022, **446**, 136904.
118 L. Jin, Y. Zheng, X. Liu, Y. Zhang, Z. Li, Y. Liang, S. Zhu, H. Jiang, Z. Cui and S. Wu, *Small*, 2022, **18**, 2204028.
119 T. Ding, F. Liu, H. Xin, Y. Chen, L. Kong, J. Han, D. Ma, Y. Han and L. Zhang, *Nano Today*, 2024, **54**, 102069.
120 J. Ye, B. Li, M. Li, Y. Zheng, S. Wu and Y. Han, *Acta Biomater.*, 2020, **107**, 313–324.
121 Y. Xu, Y. Luo, Z. Weng, H. Xu, W. Zhang, Q. Li, H. Liu, L. Liu, Y. Wang, X. Liu, L. Liao and X. Wang, *ACS Nano*, 2023, **17**, 18732–18746.
122 T. He, H. Chen, P. Liu, H. Shi, X. Xu, C. Feng, Y. Wang, X. Li, N. Lei, Y. Xiao, X. Zhu, J. Xu and X. Zhang, *J. Mater. Sci. Technol.*, 2023, **163**, 168–181.
123 Z. Wen, X. Shi, X. Li, W. Liu, Y. Liu, R. Zhang, Y. Yu and J. Su, *ACS Appl. Mater. Interfaces*, 2023, **15**, 15235–15249.
124 X. Han, G. Zhang, M. Chai and X. Zhang, *Biomed. Mater.*, 2021, **16**, 025018.
125 M.-Z. Chai, M.-W. An, X.-Y. Zhang and P.-K. Chu, *Rare Met.*, 2022, **41**, 540–545.
126 R. Lv, Y.-Q. Liang, Z.-Y. Li, S.-L. Zhu, Z.-D. Cui and S.-L. Wu, *Rare Met.*, 2022, **41**, 639–649.
127 Y.-L. Li, J. He, H.-X. Ye, C.-C. Zhao, W.-W. Zhu, X. Lu and F.-Z. Ren, *Rare Met.*, 2022, **41**, 546–558.
128 B. Li, H. Zhu, Y. Lv, C. Wang, S. Wu, S. Zhu, Y. Zheng, H. Jiang, Y. Zhang, Z. Li, Z. Cui and X. Liu, *Small*, 2023, **19**, 2303484.
129 L. Jin, S. Wu, C. Mao, C. Wang, S. Zhu, Y. Zheng, Y. Zhang, Z. Li, Z. Cui, H. Jiang and X. Liu, *Bioact. Mater.*, 2024, **31**, 284–297.
130 L. Jin, Y. Zheng, X. Liu, Y. Zhang, Z. Li, Y. Liang, S. Zhu, H. Jiang, Z. Cui and S. Wu, *Small*, 2022, **18**, 2204028.
131 F. Qi, W. Liu, Z. Li, S. Peng, Y. Chen, W. Tan and C. Shuai, *ACS Appl. Polym. Mater.*, 2024, **6**, 6581–6593.
132 W. Yang, C. Zhou, C. He, Y. Yang, W. Aiyiti, L. Xu and C. Shuai, *J. Colloid Interface Sci.*, 2025, **678**, 260–271.
133 X. Yao, D. Li, C. Gao, Y. Deng, J. Zhang and C. Shuai, *Adv. Power. Mater.*, 2024, **3**, 100216.
134 X. Tian, D. Li, Q. Lian, L. Wang, Z. Lu, K. Huang, F. Wang, Q. Liang, H. Zhang, Z. Meng, J. He, C. Sun, T. Liu, C. Huo, L. Wu and B. Lu, *Addit Manuf. Front.*, 2024, **3**, 200140.
135 D. Lin, C. Zhang, X. Chen, N. Wang and L. Yang, *Addit. Manuf. Front.*, 2024, **3**, 200123.
136 C. Ma, Q. Zeng, L. Yu, S. Yu, J. Song, Y. Ma and X. Dong, *Addit. Manuf. Front.*, 2023, **2**, 100097.
137 A. Chen, J. Su, Y. Li, H. Zhang, Y. Shi, C. Yan and J. Lu, *Int. J. Extreme. Manuf.*, 2023, **5**, 032007.
138 J. Feng, J. Fu, X. Yao and Y. He, *Int. J. Extreme. Manuf.*, 2022, **4**, 022001.
139 Z. Meng, X. Mu, J. He, J. Zhang, R. Ling and D. Li, *Int. J. Extreme. Manuf.*, 2023, **5**, 025001.
140 F. Qi, W. Liu, Y. Chen, F. Ding, W. Li, S. Peng, P. He and C. Shuai, *J. Colloid Interface Sci.*, 2025, **682**, 210–221.
141 X. Wu, J. Liu, Y. Yang, J. Bai, C. Shuai, J. Buhagiar and X. Ning, *Int. J. Extreme. Manuf.*, 2025, **7**, 022007.
142 P. Feng, R. He, F. Yang, Y. Lin, L. Fan, H. Pan and C. Shuai, *Sustainable Mater. Technol.*, 2025, **43**, e01205.
143 X. Gao, W. Deng, J. Tan, X. Shuai, J. Zan, T. Ye, K. Luo, F. Qi, Y. Wei and C. Shuai, *Mater. Today Chem.*, 2025, **43**, 102455.
144 P. Feng, L. Liu, F. Yang, R. Min, P. Wu and C. Shuai, *Biofabrication*, 2025, **17**, 012005.
145 I. Ullah, P. Ou, L. Xie, Q. Liao, F. Zhao, A. Gao, X. Ren, Y. Li, G. Wang, Z. Wu, P. K. Chu, H. Wang and L. Tong, *Acta Biomater.*, 2024, **175**, 382–394.
146 Y. Si, H. Liu, H. Yu, X. Jiang and D. Sun, *Surf. Coat. Technol.*, 2022, **431**, 128008.
147 M. Wang, J. Yao, S. Shen, C. Heng, Y. Zhang, T. Yang and X. Zheng, *Nano Res.*, 2023, **16**, 757–770.
148 H.-T. Lu, G.-Y. Huang, W.-J. Chang, T.-W. Lu, T.-W. Huang, M.-H. Ho and F.-L. Mi, *Carbohydr. Polym.*, 2022, **281**, 119035.
149 W. Chen, D. Gu, J. Yang, Q. Yang, J. Chen and X. Shen, *Int. J. Extreme. Manuf.*, 2022, **4**, 045002.
150 W. Ren, J. Xu, Z. Lian, X. Sun, Z. Xu and H. Yu, *Int. J. Extreme. Manuf.*, 2022, **4**, 015101.
151 C. Shao, H. Li, Y. Zhu, P. Li, H. Yu, Z. Zhang, H. Gleiter, A. McDonald and J. Hogan, *Int. J. Extreme. Manuf.*, 2023, **5**, 015102.
152 S. Sui, Y. Chew, F. Weng, C. Tan, Z. Du and G. Bi, *Int. J. Extreme. Manuf.*, 2022, **4**, 035102.

153 Q. Sun, Z. Xue, Y. Chen, R. Xia, J. Wang, S. Xu, J. Zhang and Y. Yue, *Int. J. Extreme. Manuf.*, 2022, **4**, 015001.
154 C. Wei, H. Gu, Y. Gu, L. Liu, Y. Huang, D. Cheng, Z. Li and L. Li, *Int. J. Extreme. Manuf.*, 2022, **4**, 025002.
155 W. Zhang, W. Hou, L. Deike and C. Arnold, *Int. J. Extreme. Manuf.*, 2022, **4**, 015201.
156 H. N. Pantaroto, A. P. Ricomini-Filho, M. M. Bertolini, J. H. D. da Silva, N. F. A. Neto, C. Sukotjo, E. C. Rangel and V. A. Barão, *Dent. Mater.*, 2018, **34**, e182–e195.
157 Y. Ma, Y.-Z. Guo, Y. Liu, Y.-R. Wang, J.-C. Yang, X.-Z. Kong, H.-L. Jia, R.-Z. Li, Q.-Z. Han, C.-D. Zheng, X.-J. Hu and B. Liu, *Front. Mater.*, 2022, **9**, 883027.
158 B. Chen, W. Wang, M. Hu, Y. Liang, N. Wang, C. Li and Y. Li, *ACS Nano*, 2024, **18**, 24968–24983.
159 T. R. Kyriakides, A. Raj, T. H. Tseng, H. Xiao, R. Nguyen, F. S. Mohammed, S. Halder, M. Xu, M. J. Wu, S. Bao and W. C. Sheu, *Biomed. Mater.*, 2021, **16**, 042005.
160 U. Theuretzbacher, K. Outterson, A. Engel and A. Karlén, *Nat. Rev. Microbiol.*, 2020, **18**, 275–285.
161 L. Mei, S. Zhu, Y. Liu, W. Yin, Z. Gu and Y. Zhao, *Chem. Eng. J.*, 2021, **418**, 129431.
162 F. J. Álvarez-Martínez, E. Barrajón-Catalán, M. Herranz-López and V. Micol, *Phytomedicine*, 2021, **90**, 153626.

